"Blind" Shape Reconstruction from Experimental Data

Peter M. van den Berg, Marc G. Coté, Member, IEEE, and Ralph E. Kleinman, Fellow, IEEE

Abstract—A method for reconstructing the shape of a bounded impenetrable object from measured scattered field data is presented. The reconstruction algorithm is, in principle, the same as that used before for reconstructing the conductivity of a penetrable object and uses the fact that for high conductivity the skin depth of the scatterer is small, in which case the only meaningful information produced by the algorithm is the boundary of the scatterer. A striking increase in efficiency is achieved by incorporating into the algorithm the fact that for large conductivity, the contrast is dominated by a large positive imaginary part. This fact together with the knowledge that the scatterer is constrained in some test domain constitute the only a priori information about the scatterer that is used. There are no other implicit assumptions about the location, connectivity, convexity, or boundary conditions. The method is shown to successfully reconstruct the shape of an object from experimental scattered field data in a "blind" test.

I. INTRODUCTION

THE present paper describes a successful example of the reconstruction of the shape of a scattering object from experimentally determined scattering data. In contrast with other inversion methods, the reconstruction is accomplished from real rather than synthetic data, so there is no chance of even inadvertently committing the "inverse crime" of using the same numerical method in the inversion algorithm as is used for solving the forward or direct problem to produce the synthetic "measured" data. The possibility of favorably prejudicing the outcome of the inversion algorithm was eliminated by a "blind" use of the measured data in the inversion algorithm; that is, knowledge of the geometry of the object from which the scattered field was measured was not supplied to those running the algorithm until after the reconstruction was completed.

The reconstruction algorithm is that described by Kleinman and Van den Berg [1] in which an iterative algorithm for the reconstruction of complex contrast profiles [2], [3] is adapted to reconstruct the shape and location of a perfectly conducting scatterer by making the assumption that the unknown contrast is essentially nonnegative imaginary. The experimental data

Manuscript received March 31, 1994; revised May 25, 1995. This work was supported by AFOSR Grant F49620-94-1-0219 and by NATO Grant 0230/88.

IEEE Log Number 9415637.

were obtained on the Ipswich Test Range of Rome Laboratories [4].

II. DESCRIPTION OF THE METHOD

A two-dimensional conducting obstacle located entirely within a test domain D is irradiated successively by J known incident fields with the electric-field vector parallel to the cylindrical object (TM-polarization). For each incident field, the nonvanishing component of the electric field is denoted by u_j^{inc} , $j=1,\cdots,J$ and the corresponding total field by u_j . The scattering object need not completely coincide with D nor is any information about the shape or location of the scatterer required other than that it lies in D. The contrast is given by

$$\chi(\mathbf{p}) = \frac{\varepsilon(\mathbf{p})}{\varepsilon_0} - 1 + i \frac{\sigma(\mathbf{p})}{\omega \varepsilon_0} \tag{1}$$

where ε_0 is the permittivity of the surrounding nonconducting medium and $\varepsilon(\boldsymbol{p})$ and $\sigma(\boldsymbol{p})$ are, respectively, the permittivity and conductivity within the scatterer and may vary with position vector \boldsymbol{p} . The contrast vanishes outside the scatterer and therefore is zero not only outside of D but also at those points in D exterior to the scatterer. The assumption that the scatterer is highly conducting is made manifest by ignoring the real part of the contrast and letting

$$\chi(\mathbf{p}) = i\zeta^2(\mathbf{p}) \tag{2}$$

for real ζ , which guarantees that the contrast is positive imaginary. For each u_j^{inc} , the scattered field is measured on a surface S which encloses the test domain D, and the measured values are denoted by $f_j(\boldsymbol{p})$, $\boldsymbol{p} \in S$. In principle, D may be any domain enclosing the scatterer and S any surface exterior to D, but in the present case D was taken to be a square and S was a circle of radius sufficiently large not only so that S contained D, but also to justify the far-field approximation for the scattered field.

The conductivity reconstruction problem is that of finding $\zeta(p)$ for known u_j^{inc} and measured f_j . If ζ is very large, the boundary of the scatterer is the only meaningful information that may be obtained from the reconstruction. The method employed here to achieve this reconstruction problem utilizes both the integral equations

$$u_{j}(\mathbf{p}) + \frac{k^{2}}{4} \int_{D} H_{0}^{(1)}(k|\mathbf{p} - \mathbf{q}|) \zeta^{2}(\mathbf{q}) u_{j}(\mathbf{q}) dv_{\mathbf{q}} = u_{j}^{inc}(\mathbf{p}),$$

$$\mathbf{p} \in D$$
 (3)

P. M. van den Berg is with the Laboratory of Electromagnetic Research, Faculty of Electrical Engineering, Delft University of Technology, Delft, The Netherlands.

M. G. Coté is with the Rome Laboratory/ERCT, Hanscom AFB, MA 01731-5000 USA.

R. E. Kleinman is with the Center for the Mathematics of Waves, Department of Mathematical Sciences, University of Delaware, Newark, DE 19716

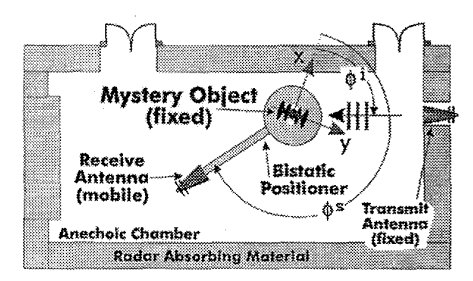


Fig. 1. Schematic diagram of the automated swept-angle bistatic measure-

and the integral representations

the integral representations
$$u_j^{sct}(\boldsymbol{p}) = -\frac{k^2}{4} \int_D H_0^{(1)}(k|\boldsymbol{p}-\boldsymbol{q}|) \, \zeta^2(\boldsymbol{p}) \, u_j(\boldsymbol{q}) \, dv_{\boldsymbol{q}},$$

$$\boldsymbol{p} \in S.$$
 (4)

Here, k is the wavenumber, and p and q are two-dimensional position vectors. With the scattered fields u_i^{sct} replaced by the measured data f_j , sequences of functions $\{u_{j,n}\}_{n=0}^N$ and $\{\zeta_n\}_{n=0}^N$ are constructed iteratively to successively reduce the error in satisfying the two sets of integral relations, (3) and (4). Actually, these equations are discretized by subdividing D into subsquares and choosing both u_i and ζ to be constant on each subsquare. The details of the starting values $u_{i,0}$ and ζ_0 and construction of the sequences are given in [1].

III. EXPERIMENTAL SETUP

Here we describe how the field scattered by the mystery object was measured and calibrated for the reconstruction. The measurement frequency was 10.0 GHz, thus the wavelength (λ) was 3 cm. Bistatic scattering measurements were made in a plane perpendicular to the axis of the cylindrical object 30 cm (10 λ) in length, and the measurement plane intersected at mid length. For convenience, a Cartesian coordinate system was oriented with z along the cylinder axis, and measurements were made in the (x, y) plane. The measurement configuration is shown in Fig. 1. The scattered fields were collected for incident angles of $\phi^i = \{0, 5, 10, 15, 20, 45, 60, 90\}$ degrees, over the observation sector $0 \le \phi^s \le 359.5$ degrees with a sample spacing, $\Delta \phi^s = 0.5$ degrees. At present, only data for these nonuniformly spaced incident angles are available.

The object and transmit antenna were fixed for each ϕ^i , and the receive antenna was rotated on a semi-circular arc about the object from back scatter to forward scatter recording the total field coincident with the receive antenna polarization. A second measurement was made with the object removed. This background field measurement was subtracted from each of the total-field measurements to obtain measured data proportional to the scattered field. The range from the transmit antenna to the object was 3.7 m, and the range from the object to the receive antenna aperture was 2.8 m. Both the source and the probe antennas had circular apertures 15.24 cm in diameter. With these measurement ranges and antennas, the object illumination was uniform in magnitude to within 0.2 dB along the x-direction and 1 dB along the z-direction. The illumination phase taper over the object was approximately 10 degrees and 50 degrees in the x- and z-directions, respectively. We note that both the end sides $(z = \pm 15 \text{ cm})$ of the finite cylindrical object were illuminated quite strongly, and therefore one might expect the measured scattered field would contain an undesirable diffraction from the edges of the end sides. In this experiment, however, the planes of incidence and observation were always normal to the z-axis which ensured that the scattered field was dominated by the specular response, and the diffraction from the two truncating sides, being much less, was not observable. Thus, the measured scattering from the finite cylindrical object was very close to that from an infinite cylindrical object.

The measurement system used can only scan over a 190degree bistatic angular sector. This means that to get scattering data over a complete 360-degree bistatic observation sector, two measurement runs had to be made for each incident direction, one measurement run to cover the observation sector, $\phi^i - 5$ degrees $\leq \phi^s \leq \phi^i + 185$ degrees and the other to cover $\phi^i + 175$ degrees $\leq \phi^s \leq \phi^i + 365$ degrees. The data from each measurement run must be independently calibrated and then spliced together to make a complete data set. In this experiment, coverage of the first observation sector for every incident angle of interest (except $\phi^i = 0$), was accomplished by measurements made in March of 1990. The second observation sector was obtained for all incident angles of interest (except $\phi^i = 90$ degrees), by measurements made in October of 1991. The instrumentation radar used in the October 1991 measurements was more sensitive than the radar used in the March 1990 measurements so that the March portion of each complete data set had an uncertainty significantly greater than the October portion. In addition to a variable uncertainty, each data set contained a sector of completely erroneous scattering centered about the backscattering direction (ϕ^i -5 degrees $\leq \phi^s \leq \phi^i + 5$ degrees) caused by the interruption of the object illumination when the receive antenna passed between the transmit antenna and object. For each measurement run we filled in the erroneous back-scattering region by extrapolating the complex data on ϕ^i +5 degrees $\leq \phi^s \leq \phi^i$ + 185 degrees, using a least squares linear prediction algorithm [5].

The raw scattering data, resulting from the phasor subtraction of the total-field and background measurements, has a magnitude proportional to the object scattering cross section per unit length and a phase proportional to the phase of the scattered electric field referenced to the center of rotation of the bistatic positioner. Aligning the object so that its symmetry axis coincides with this rotation axis is practically impossible. Our calibration procedure must compensate for the phase error caused by this misalignment in addition to calibrating the magnitude. We calibrated the scattering from the object by the following procedure. We computed a point calibration phasor

$$\Psi(\phi^s) = \frac{\pi}{2\lambda} \frac{P^{comp}(\phi^s)}{P^{exp}(\phi^s)}.$$
 (5)

In (5), $P^{exp}(\phi^s)$ is the measured scattered pattern of the object for a particular measurement run and $P^{comp}(\phi^s)$ is the far-field scattering pattern computed for an infinitely long cylinder that approximates the present object but with its symmetry axis at

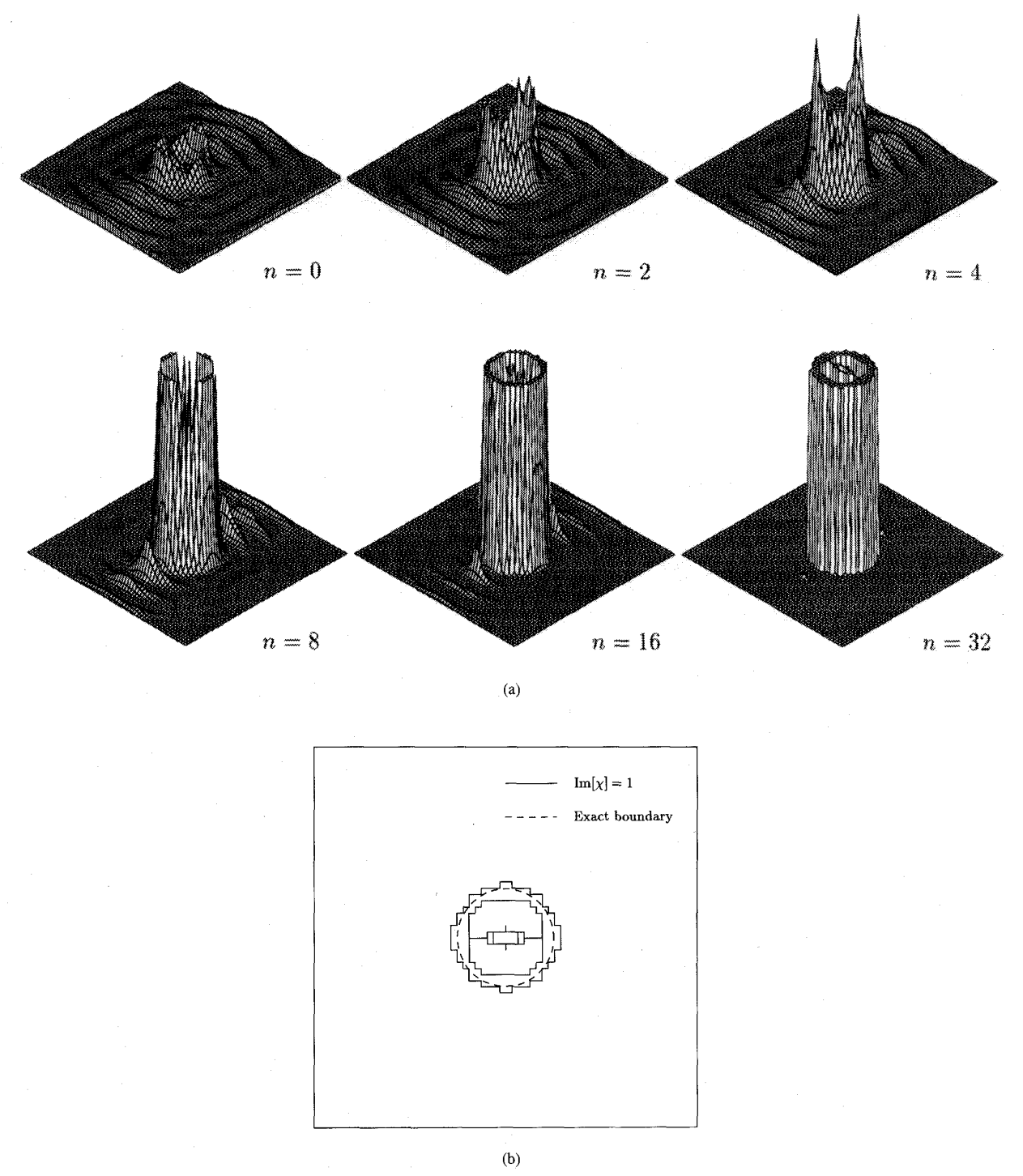


Fig. 2. (a) The reconstructed imaginary values of the contrast from synthetic data. (b) Comparison between the reconstructed boundary and the exact one (synthetic data, n=32).

the z-axis. From the calibration phasor we compute an average calibration factor, Ψ_0 , and three constants, $a,\ b,$ and c. The average calibration factor is defined as

$$\Psi_0 = \frac{1}{N} \sum_{n=1}^{N} \left| \Psi(n\Delta\phi^s + \phi^i + 5 \text{ degrees}) \right| \tag{6}$$

where N is the number of data points in the given measurement run excluding the erroneous data in the 10-degree back-scattering sector. The three constants are determined such that they produce the best fit (in the least square sense) to the expression

$$\arg\left[\Psi(\phi^s)\right] = a + b\cos(\phi^s + c) . \tag{7}$$

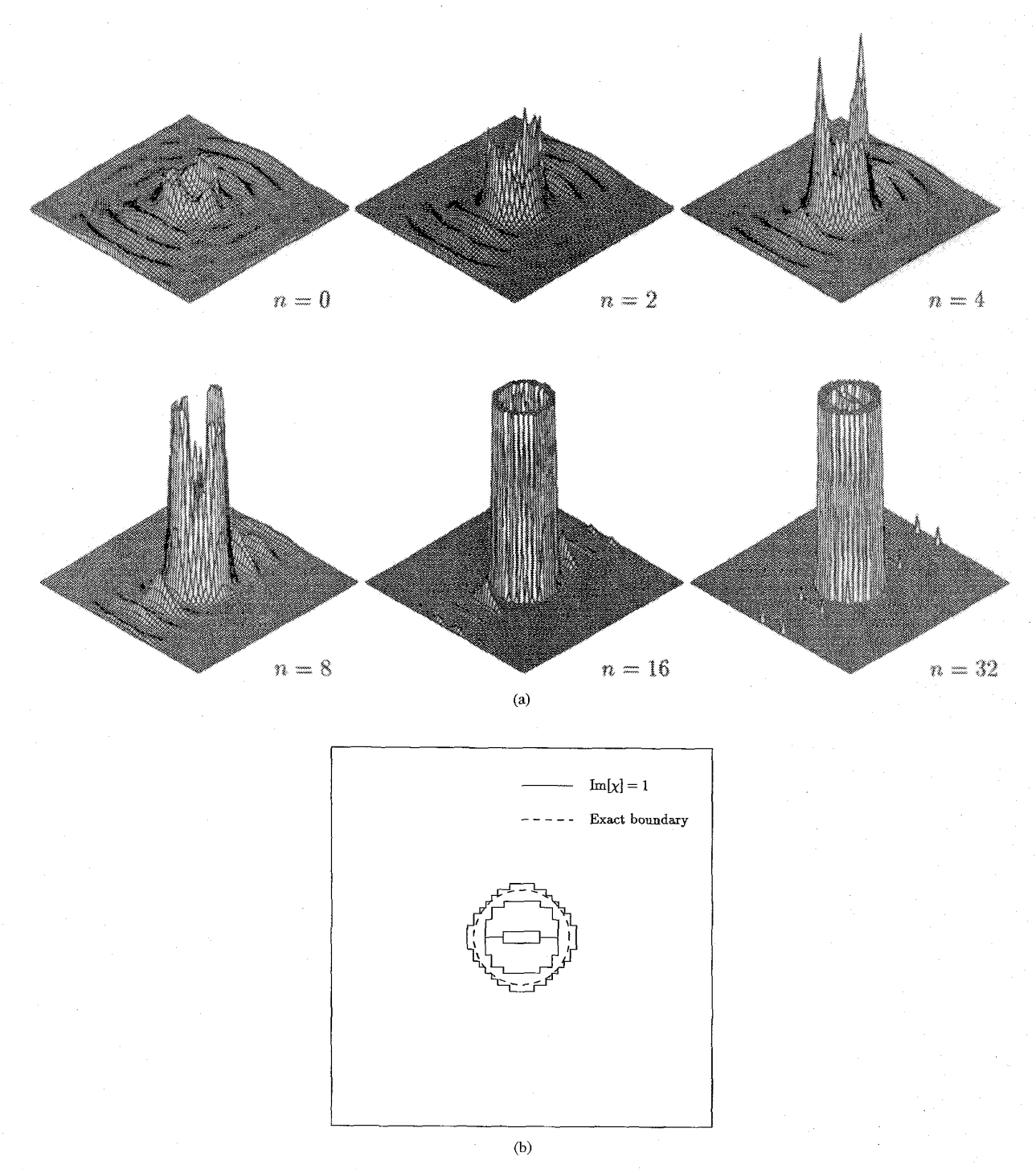


Fig. 3. (a) The reconstructed imaginary values of the contrast from experimental data. (b) Comparison between the reconstructed boundary and the exact one (experimental data, n = 32).

This curve fitting step is needed to correct for the misalignment phase error (see [4] for a more thorough discussion). With those four constants computed for each measurement run, the calibrated scattering cross section per unit length, $\sigma^{cal}(\phi^s)$, was calculated from the relation

$$\sigma^{cal}(\phi^s) = \Psi_0 P^{\exp}(\phi^s) \exp\left\{-i[a+b\cos\left(\phi^s+c\right)]\right\}. \quad (8)$$

In this way we have arrived at experimental data that belongs to the object with the symmetry axis coinciding with the z-axis. We note that this procedure was necessary because we have only angles of incidence in a quarter plane, and using the symmetry, we can obtain scattered data from angles of incidence in the full plane. These experimental data are recalibrated for use in the inversion algorithm as described in the next section.

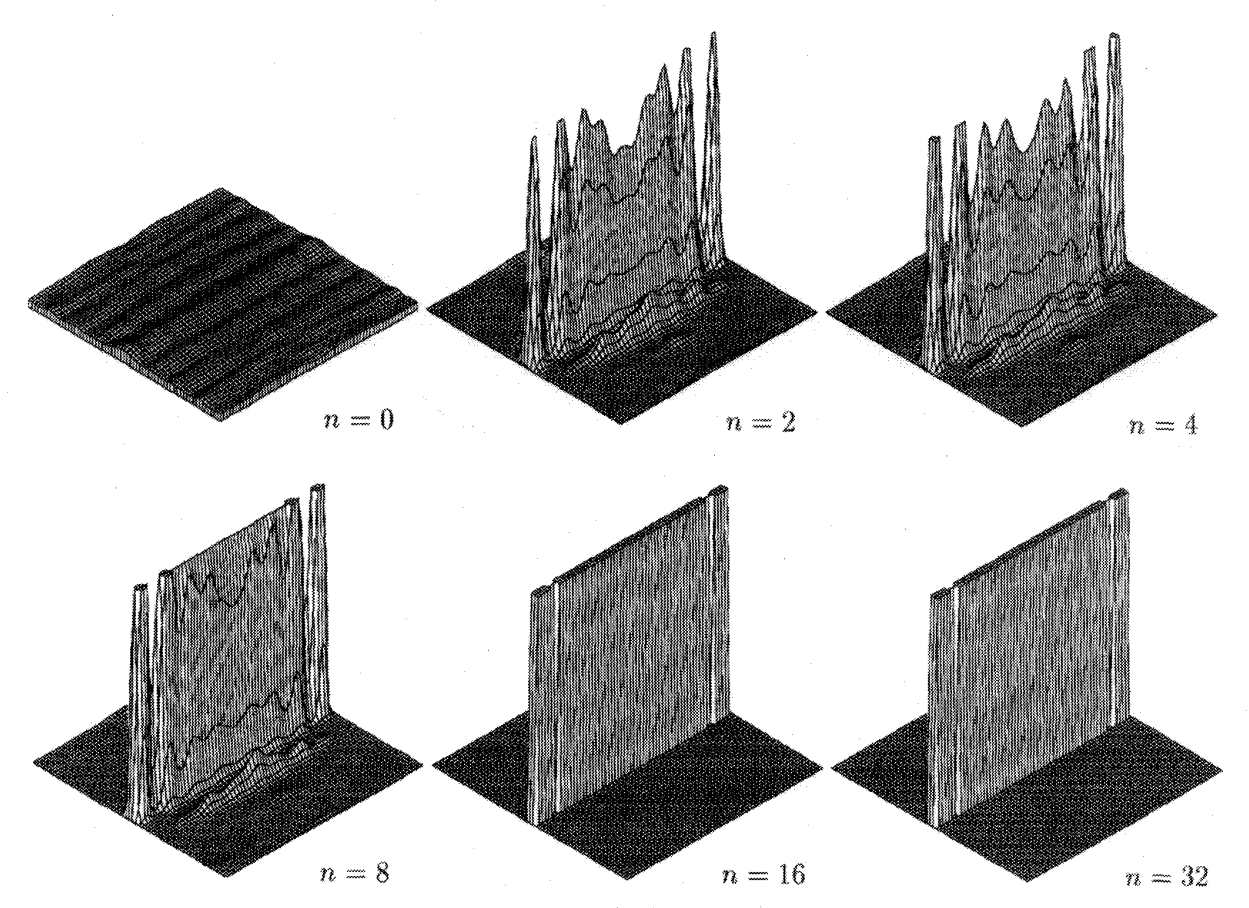


Fig. 4. The reconstructed imaginary values of the contrast of the mystery object (dimension of test domain = 0.126×0.126 m²).

IV. RECONSTRUCTION

The measurement surface S is chosen to be a circle containing the test domain. We assume that the radius of this circle is large enough so that the far-field approximation of (4) may be employed, and the far-field coefficient is the quantity of interest so that the dependence on the radius is removed. In that case the data may be written as

$$f_j(\mathbf{p}) \sim \frac{i}{4} \left(\frac{2}{\pi k |\mathbf{p}|}\right)^{\frac{1}{2}} \exp(ik|\mathbf{p}| - i\frac{\pi}{4}) f_j^{\infty}(\hat{\mathbf{p}})$$
 (9)

and (4) may be replaced by

$$f_j^{\infty}(\hat{\boldsymbol{p}}) = i \int_D \exp(-ik\hat{\boldsymbol{p}} \cdot \boldsymbol{q}) \zeta^2(\boldsymbol{q}) u_j(\boldsymbol{q}) dv_{\boldsymbol{q}} , \quad \hat{\boldsymbol{p}} \in S \quad (10)$$

where \hat{p} is the unit vector in the direction of observation and S now denotes the space of these unit vectors, the unit circle. Further, $f_j^{\infty}(\hat{p})$ are the measured far-field data. In the examples, we take from the measured far-field data the values at 36 angles equally spaced around the object (the domain S consists of 36 discrete points \hat{p}_l). In the experiments only eight excitations are carried out. The incident fields are approximated as plane waves incident at an angle of 0, 5, 10, 15, 20, 45, 60 and 90 degrees with the x-axis, respectively. To obtain scattered-field data from incident waves

distributed around the object, we take advantage of the *a priori* information that the mystery object is symmetric with respect to the planes x = 0 and y = 0. Doing so, we obtain scattered-field data from 28 excitations (J = 28).

Further, we have a priori information that the mystery object lies inside a circle with a radius of 0.060 m, and the frequency of operation is 10 GHz. We therefore will assume that the object is located inside a test square divided into 63×63 subsquares of 0.002×0.002 m². The discretized version of the algorithm is discussed in [1].

Calibration

To test the computer code, we first run the algorithm for synthetic data obtained in the well-known problem of scattering of a plane wave by a perfectly conducting circular cylinder with origin at the center of the test square. We employ the same angles of incidence and data points as used in the experimental case. The analytic solution in terms of Bessel functions has been employed. The data are denoted as

$$f_i^{anl}(\hat{\mathbf{p}}_l) := f_i^{\infty}(\hat{\mathbf{p}}_l), \quad j = 1, \dots, 28, \quad l = 1, \dots, 36.$$
 (11)

The radius, a, of this circular cylinder is 0.0159 m. The wavelength is $\lambda = 0.030$ m, so that $ka = \pi$. We have seen that our scheme indeed reconstructs the location and the shape of a

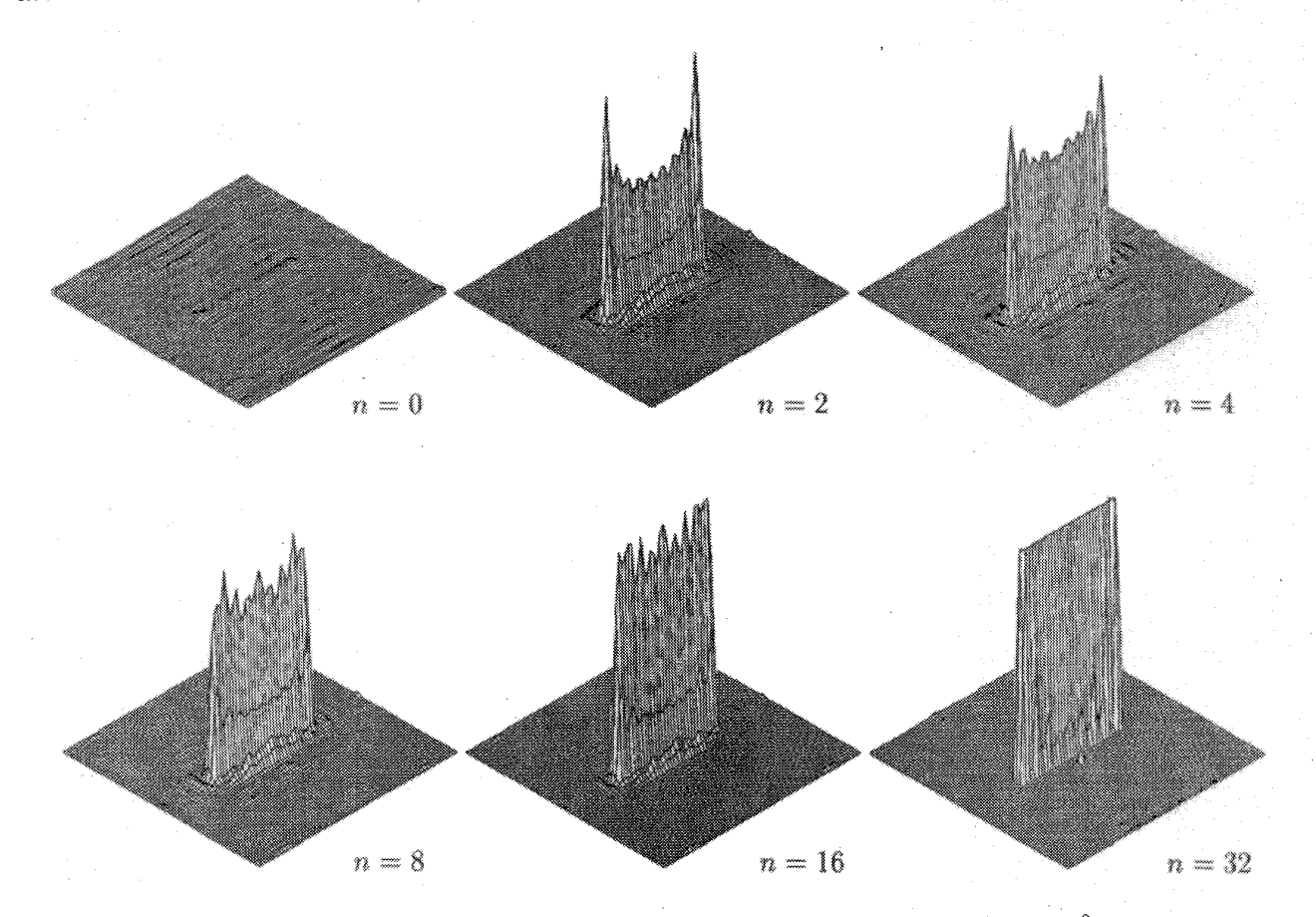


Fig. 5. The reconstructed imaginary values of the contrast of the mystery object (dimension of test domain = 0.252×0.252 m²).

perfectly conducting cylinder by reconstructing the imaginary contrast at the boundary [1]. The reconstructed contrast at the boundary becomes highly oscillatory, however, after a couple of iterations. The peaks appear to increase with the number of iterations and it becomes difficult to choose the level value of the contour that estimates the boundary of the object. The visualization of the boundary of the object is improved when we impose an upper bound to the reconstructed contrast. If at some point in the iteration the reconstructed ζ_n is larger than ζ_{max} , the contrast is replaced by ζ_{max} . In our example we take $\zeta_{max} = 1$. Some surface plots of the reconstructed profiles (the imaginary part of the contrast, $\text{Im}[\chi] = \zeta^2$) from the synthetic data of the circular cylinder are presented in Fig. 2(a). The result at 32 iterations has also been presented in Fig. 2(b) where we have plotted the boundaries of the test domain and the contour lines $\zeta = 1$. The exact location of the boundary of the object is indicated by the dashed circle. The asymmetry of the choice of the incident angles of excitations is clearly visible in the reconstructed boundary. We observe that the boundary is located with an error of the sample width.

Next we measure experimentally the scattering from a circular cylinder with the same dimensions. These data are denoted as $f_j^{exp}(\hat{\mathbf{p}}_l)$, $j=1,\cdots,28$, $l=1,\cdots,36$. To calibrate an overall phase shift between the definition of the phase of the measurement data and the one defined in the reconstruction

scheme (and to some extent the amplitudes), we assume that the measured signal is a correct part of a multiplicative complex factor and enforce the data to be

$$f_j^{cal}(\hat{\mathbf{p}}_l) := C f_j^{exp}(\hat{\mathbf{p}}_l), \quad j = 1, \cdots, 28, \quad l = 1, \cdots, 36.$$
 (12)

The constant C is determined from the analytical data pertaining to this object by minimizing the deviation

$$\sum_{j=1}^{J} |f_{j}^{anl}(\hat{\mathbf{p}}) - C f_{j}^{exp}(\hat{\mathbf{p}})|_{S}^{2}$$

$$= \sum_{j=1}^{36} \sum_{l=1}^{28} |f_{j}^{anl}(\hat{\mathbf{p}}_{l}) - C f_{j}^{exp}(\hat{\mathbf{p}}_{l})|^{2}$$
(13)

resulting in

$$C = \frac{\sum_{j=1}^{J} \langle f_{j}^{anl}(\hat{\boldsymbol{p}}), f_{j}^{exp}(\hat{\boldsymbol{p}}) \rangle_{S}}{\sum_{j=1}^{J} \|f_{j}^{exp}(\hat{\boldsymbol{p}})\|_{S}^{2}} = \frac{\sum_{j=1}^{36} \sum_{l=1}^{28} f_{j}^{anl}(\hat{\boldsymbol{p}}_{l}) \overline{f_{j}^{exp}(\hat{\boldsymbol{p}}_{l})}}{\sum_{j=1}^{36} \sum_{l=1}^{28} |f_{j}^{exp}(\hat{\boldsymbol{p}}_{l})|^{2}}$$
(14)

where the overbar denotes a complex conjugate. After substitution of the resulting numerical value of C into the deviation

of (13), we found that

$$\left[\frac{\sum_{j=1}^{J} \|f_{j}^{anl}(\hat{\boldsymbol{p}}) - C f_{j}^{exp}(\hat{\boldsymbol{p}})\|_{S}^{2}}{\sum_{i=1}^{J} \|f_{j}^{anl}(\hat{\boldsymbol{p}})\|_{S}^{2}} \right]^{\frac{1}{2}} = 0.079$$
(15)

that is, a mean square deviation of about 8%. Using these recalibrated data, we ran the inversion algorithm. Some surface plots of the reconstructed profiles (the imaginary part of the contrast, $\text{Im}[\chi] = \zeta^2$) from these calibrated experimental data of the circular cylinder are presented in Fig. 3. The result at 32 iterations has also been presented in Fig. 3(b) where we have plotted the boundaries of the test domain and the contour lines $\zeta=1$. The reconstruction from our experimental data is not very different from the reconstruction using the synthetic data. Furthermore, it is noted that increasing the number of iterations does not eliminate the artifacts in the center of the reconstructed contrast.

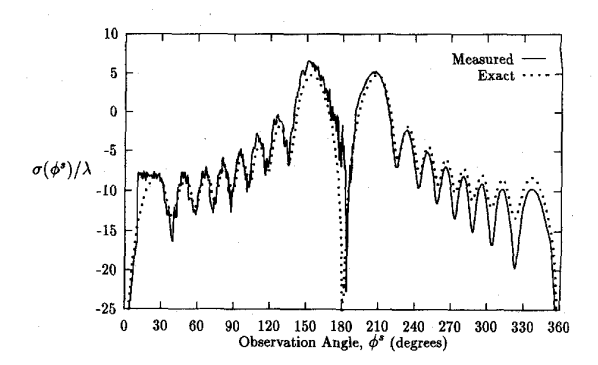
Mystery object

Observing that our reconstruction of the circular cylinder was successful, we now continue to reconstruct a mystery object from experimental data. The experimental data from this mystery object were first multiplied with the complex constant C, computed by minimizing the global deviation between analytical and experimental data from the circular-cylinder case. This ensures that an overall phase shift between the one defined in the measurements and the one in the reconstruction scheme is corrected. We then run the inversion algorithm and the results of the reconstruction are shown in Fig. 4. It clearly shows that the mystery object is probably a strip of about a width of 12 cm and a thickness of less than or equal to 4 mm.

Finally, we show in Fig. 5, the reconstruction in a larger test domain divided into 63×63 subsquares of 0.004×0.004 m². The result of the reconstruction, using this coarser grid, is consistent with the previous result.

After this reconstruction, the mystery was revealed to those running the reconstruction algorithm: the object is a 10 λ long (30 cm), 4 λ (12 cm) wide, and 0.106 λ (0.32 cm) thick aluminum plate. Obviously, the cross-sectional dimensions of the mystery object that are obtained from the reconstruction results are very close to the real ones.

To show the quality of the measurements, we have computed the far-field data of the infinitely long and infinitely thin strip using the eigenfunction expansions described by Asvestas and Kleinman [6]. In Fig. 6 we compare the computed results of the strip with the measured results of the plate for one incidence direction (ϕ^i =10 degrees). Notice that the measured scattering from about 5 degrees off back scatter (ϕ^s = 15 degrees) to about ϕ^s =190 degrees is noisier than the remainder of the curve. The noisy sector corresponds to the measurements made in March of 1990. In addition, notice that the measured curve near $\phi^s = \phi^i = 10$ degrees is flat and does not match the exact curve. This is the back-scattering region that contains the extrapolated data.



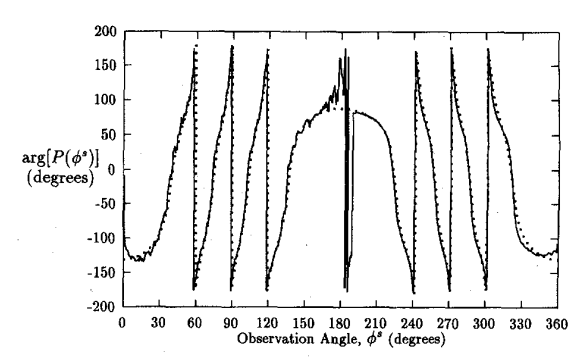


Fig. 6. Bistatic scattering from the 4λ strip illuminated 10 degrees off grazing (TE-polarization).

V. CONCLUSIONS

This paper presents definitive evidence of the effectiveness of the modified gradient inverse scattering algorithm in reconstructing the shape of a perfectly conducting cylindrical object of arbitrary cross section from scattered field data. In earlier papers it was shown that the algorithm was effective in reconstructing the contrast of penetrable objects, the boundary of impenetrable circular cylinders, and was stable with respect to white noise. All previous tests were performed with synthetic, i.e., computer simulated, scattering experiments and thus were not free from the possibility that they were tainted by an "inverse crime" of somehow using knowledge of the scatterer to favorably influence the reconstruction. The present results show conclusively that the algorithm will yield a successful reconstruction when the data are obtained experimentally and the shape of the object was not known before the reconstruction was completed, thus removing any question that an "inverse crime," however inadvertent, was committed. These results describe only one scattering experiment and additional experiments are needed, not only to reconfirm the present results, but also to test the effectiveness of the reconstruction algorithm for penetrable scatterers.

REFERENCES

- [1] R. E. Kleinman and P. M. van den Berg, "Two-dimensional location and shape reconstruction," *Radio Sci.*, vol. 29, pp. 1157–1169, July-Aug. 1994
- [2] _____, "A modified gradient method for two-dimensional problems in tomography," J. Computational Applied Math., vol. 42, pp. 17–35, 1992.
- [3] _____, "An extended range modified gradient technique for profile inversion," *Radio Sci.*, vol. 28, pp. 877–884, Sep.-Oct. 1993.

- [4] M. G. Coté, "Automated swept-angle bistatic scattering measurements using continuous wave radar," *IEEE Trans. Instrum. Meas.*, vol. 41, pp. 185–192, Apr. 1992.
- [5] S. L. Marple, Jr., Digital Spectral Analysis. Englewood Cliffs, NJ: Prentice-Hall, 1987, chap. 8.
 [6] J. S. Asvestas, and R. E. Kleinman, "The strip," chap. 4 in Electromag-
- [6] J. S. Asvestas, and R. E. Kleinman, "The strip," chap. 4 in *Electromagnetic and Acoustic Scattering by Simple Shapes*, J. J. Bowman, T. B. A. Senior, P. L. E. Uslenghi, Eds. Amsterdam: North-Holland, 1969.



Peter M. van den Berg was born in Rotterdam, The Netherlands, on November 11, 1943. He received the degree in electrical engineering from the Polytechnical School of Rotterdam in 1964, the B.Sc. and M.Sc. degrees in electrical engineering, and the Ph.D. degree in technical sciences, all from the Delft University of Technology, in 1966, 1968, and 1971, respectively.

From 1967 to 1968, he was employed as a Research Engineer by the Dutch Patent Office. Since 1968, he has been a member of the Scientific Staff

of the Electromagnetic Research Group of the Delft University of Technology. During these years he carried out research and taught classes in the area of wave propagation and scattering problems. During the academic year 1973-1974 he was a Visiting Lecturer in the Department of Mathematics, University of Dundee, Scotland. During a three month period during 1980-1981, he was a Visiting Scientist at the Institute of Theoretical Physics, Goteborg, Sweden. He was appointed as full Professor at the Delft University of Technology in 1981. At present, his research interest is the efficient computation of field problems using iterative techniques based on error minimization, both for the forward scattering problem and the inverse scattering problem as well as the use of wave phenomena in seismic data processing.



Marc G. Coté (S'85-M'85) was born in Lewiston, ME, on September 4, 1959. He received the BSEE and MSEE degrees, both from the University of Maine, Orono, in 1982 and 1989, respectively.

Since 1983 he has been with the Rome Laboratory (formerly Rome Air Development Center). Electromagnetics and Reliability Directorate, Bedford, MA, as a Research Engineer in the Target Characterization group. His research interests include bistatic scattering measurement techniques, nearfield measurement techniques, and electromagnetic

scattering simulations.

Mr. Coté is a member of the Antenna Measurements Techniques Associ-



Ralph E. Kleinman (M'75–SM'83–F'94) was born in New York in 1929. He received the BA degree from New York University, in 1950, the MA degree from the University of Michigan, Ann Arbor, in 1951, and the Ph.D. degree from the Delft University of Technology in the Netherlands, in 1961, all in mathematics.

He was a permanent member of the Radiation Laboratory at the University of Michigan from 1951 until 1968 when he joined the Department of Mathematical Sciences at the University of Delaware

where he is currently a Professor and Director of the Center for the Mathematics of Waves. He has held visiting positions at the Technical University of Denmark, University of Strathclyde, Delft University of Technology, AFCRL (now Rome Laboratory), University of Gottenburg, David Taylor Naval Ship Research and Development Center, the Naval Research Laboratory, University of Paris VI, Ecole Superieure d'Electricité, CNRS, and the University of Nice, Sophia Antipolis. His research interests have included the mathematical problems associated with propagation and scattering of acoustic and electromagnetic waves including radar cross-section analysis, integral representations of solutions of the Helmholtz and Maxwell equations, and low frequency perturbation techniques, as well as inverse scattering and iterative solutions of integral equations.

Dr. Kleinman now serves as an Associate Editor of SIAM Journal of Applied Mathematics and has been an Associate Editor of Radio Science and Inverse Problems and is a past chair of the U.S. Commission B of URSI.